Environmental Science & Technology

Article

pubs.acs.org/est

# Dependence of Soot Optical Properties on Particle Morphology: Measurements and Model Comparisons

James G. Radney,[†,‡] Rian You,[†,‡] Xiaofei Ma,[†,‡] Joseph M. Conny,[†] Michael R. Zachariah,[†,‡] Joseph T. Hodges,[†] and Christopher D. Zangmeister*[,†]

[†]Material Measurement Laboratory, National Institute of Standards and Technology, Gaithersburg, Maryland 20899, United States

[‡]Department of Mechanical Engineering and Department of Chemistry and Biochemistry, University of Maryland, College Park, Maryland 20742, United States

Supporting Information

**ABSTRACT:** We report the first mass-specific absorption and extinction cross sections for size- and mass-selected laboratory-generated soot aerosol. Measurement biases associated with aerosols possessing multiple charges were eliminated using mass selection to isolate singly charged particles for a specified electrical mobility diameter. Aerosol absorption and extinction coefficients were measured using photoacoustic and cavity ring-down spectroscopy techniques, respectively, for lacey and compacted soot morphologies. The measurements show that the mass-specific absorption cross sections are proportional to particle mass and independent of morphology, with values between 5.7 and 6 $m^2\ g^{-1}$. Mass-specific extinction cross sections were morphology dependent and ranged between 12 and 16 $m^2\ g^{-1}$ for the lacey and compact morphologies, respectively. The resulting single-scattering albedos ranged from 0.5 to 0.6. Results are also compared to theoretical calculations of light absorption and scattering from simulated particle agglomerates. The observed absorption is relatively well modeled, with minimum differences between the calculated and measured mass absorption cross sections ranging from ~5% (lacey soot) to 14% (compact soot). The model, however, was unable to satisfactorily reproduce the measured extinction, underestimating the single-scattering albedo for both particle morphologies. These discrepancies between calculations and measurements underscore the need for validation and refinement of existing models of light scattering and absorption by soot agglomerates.

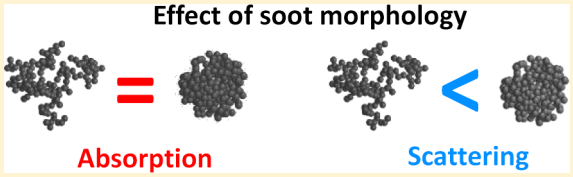


## INTRODUCTION

Many optical measurements of size selected aerosols using a differential mobility analyzer are biased by the presence of multiply charged, larger particles possessing an equivalent electrical mobility diameter to the particle of interest.[1−5] The recent publication of a method to eliminate multiply charged particles by mass-based separation both reduces uncertainty through elimination of the above bias and allows the aerosol electrical mobility diameter and mass to be known.[6] These optical measurements can be directly tied to global climate models that require the combination of aerosol mass specific absorption cross section (MAC, $m^2\ g^{-1}$), mass specific scattering cross section (MSC), mass specific extinction cross section (MEC), and single scattering albedo ($\omega_0$) as inputs. Given that extinction is the sum of absorption and scattering, and albedo is the ratio of scattering to extinction, then

$$\omega_0 = \frac{\mathrm{MSC}}{\mathrm{MAC} + \mathrm{MSC}} = \frac{\mathrm{MSC}}{\mathrm{MEC}} \quad (1)$$

Here MAC represents the mass specific absorption cross section

$$\mathrm{MAC} = \frac{\alpha_{\mathrm{abs}}}{m_p \cdot N} = \frac{C_{\mathrm{abs}}}{m_p} \quad (2)$$

where $N$ and $m_p$ are the number density, and average mass of the particles, respectively, and $C_{\mathrm{abs}}$ ($m^2$) is the particle absorption cross section. The term $\alpha_{\mathrm{abs}}$ ($m^{-1}$) is the absorption coefficient, which is the fractional loss in light intensity per-unit-propagation distance and is equal to the product $N \cdot C_{\mathrm{abs}}$. Analogous equations for MSC (scattering) and MEC (extinction) can be defined by replacing the pair ($\alpha_{\mathrm{abs}}$, $C_{\mathrm{abs}}$) in eq 2, with ($\alpha_{\mathrm{sca}}$, $C_{\mathrm{sca}}$) and ($\alpha_{\mathrm{ext}}$, $C_{\mathrm{ext}}$), respectively. In this study, we apply the above-described technique to measure *in situ* the optical morphology dependence of soot, where isolation of singly charged particles has proven challenging, potentially compromising previous measurements.

The optical properties of black carbon (BC) and soot aerosols are of significant importance as these species have been recognized as the greatest anthropogenic aerosol contributors to global warming.[7−9] Both species exhibit brief atmospheric lifetimes, and their reduction offers a potential strategy for rapid mitigation of global warming caused by long-lived gas-phase species.[7]

Received: September 19, 2013
Revised: February 11, 2014
Accepted: February 18, 2014
Published: February 18, 2014

   dx.doi.org/10.1021/es4041804 | Environ. Sci. Technol. 2014, 48, 3169−3176

Various nomenclatures exist to describe atmospheric aerosols that strongly absorb light. For consistency and clarity, we use the following definitions proposed in Buseck et al. (2012)[8] to distinguish between BC and soot. Black carbon is composed primarily of elemental carbon (EC) with a graphitic structure and exhibits strong light absorption with near $\lambda^{-1}$ power law dependence,[9] low chemical reactivity and high thermal stability,[10,11] whereas soot is more generally a mixture of EC and organic carbon (OC) having an amorphous graphitic structure with small amounts of hydrogen and oxygen present as phenolic and carboxylic groups.[10−12] Soot can contain both a strongly absorbing EC component and a weakly absorbing OC component, and the ratio of EC to OC in soot affects its light absorption and scattering properties.[13,14]

This investigation focuses on soot, which is a byproduct of the incomplete combustion of hydrocarbons that condense to form monomers with diameters between 10 and 100 nm that have an inner core surrounded by an outer shell.[8] The core can be hollow[15] or consist of several smaller particles that are a few nm in diameter[12] that can be coated with OC.[8] Absorption and scattering by a soot monomer can vary by more than an order of magnitude; both are a function of monomer diameter and molecular composition. Soon after formation the monomers form aggregates. Multiple aggregates then assemble into a single particle with an open, lacey morphology.

The morphology of soot can change through water adsorption and/or evaporation, reaction with trace gases, or agglomeration with other particles to result in compacted, spherical particles. Several modeling studies have predicted that the optical properties of soot are highly dependent on morphology; albeit with inconstant results.[16−19] However, experimental measurements have yet to confirm the morphological dependence of bare soot.

The structure of soot is well described by[16,20]

$$N_{mon} = k_0\left(\frac{2R_g}{D_{mon}}\right)^{D_f} \quad (3)$$

where $N_{mon}$ is the number of primary monomers, $k_0$ is the fractal prefactor, $R_g$ is the radius of gyration, $D_{mon}$ is the diameter of a monomer, and $D_f$ is the fractal dimension. Particle morphology is a function of $D_f$ with values ranging between 3 for spherical particles and unity for a linear chain. A fractal dimension of 1.8 is commonly assumed for fresh soot.[9] Particle packing density and aspect ratio are functions of $k_0$.[21]

The morphology of soot can also be quantified using a mass-mobility power-law relationship.[22] For a particle of mass $m_p$ and electrical mobility diameter, $D_m$, we use the expression

$$m_p = m_{p,0}\left(\frac{D_m}{D_{m,0}}\right)^{D_{fm}} \quad (4)$$

where $m_{p,0}$ corresponds to the particle mass for an arbitrarily chosen mobility diameter $D_{m,0}$ and $D_{fm}$ is the mass versus mobility diameter scaling exponent where the exponent is a surrogate for fractal dimension;[23,24] however, $D_f$ and $D_{fm}$ are not directly interchangeable.[25] A similar relationship between aggregate sphere equivalent volume and monomer diameter has also been presented.[1] Using a tandem differential mobility analyzer (DMA), aerosol particle mass analyzer (APM) and condensation particle counter (CPC), $D_m$ and the corresponding $m_p$ can be measured allowing for calculation of $m_{p,0}$ and $D_{fm}$ from a log−log fit.[23]

In the remainder of this Article, we investigate if the measured mass specific absorption and extinction cross sections of bare soot depend on particle morphology. We used a well-characterized diffusion flame burner to prepare freshly emitted soot with a lacey morphology. We also tune the soot morphology from the lacey to a compacted state using $H_2O$ uptake and rapid removal, as previously described.[26] Using electrical mobility and mass selection, the mass specific absorption and extinction cross sections were measured in manner similar to previously described.[6] These measured data are then compared to values calculated using the superposition T-matrix method to determine if the model is capable of reproducing the measured mass specific cross sections and trends.

## MATERIALS AND METHODS

**Experimental Configuration.** The reported measurements of lacey and compact soot aggregates involved three main steps as indicated in Figure 1. These include (1) aerosol generation and conditioning, (2) size and mass selection, and (3) *in situ* particle analysis.

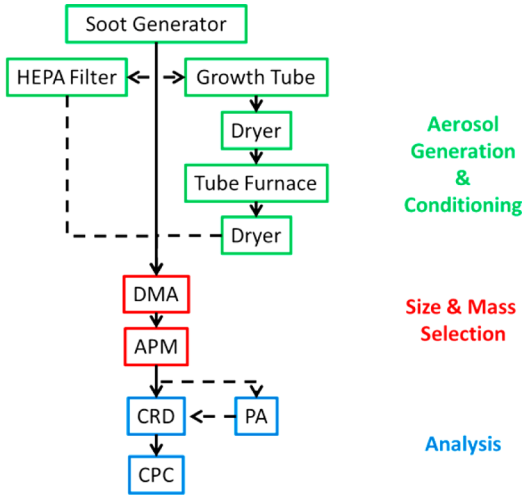


**Figure 1.** Schematic diagram of the system used to generate soot aerosol, tune its morphology, size, and mass select particles and measure absorption or extinction and number density. HEPA filter was included to collect background optical measurements. Dashed lines indicate optional flows.

In the first step, soot was generated using a Santoro-style diffusion burner operating using ethylene fuel.[1,27] The soot was aspirated into a dry, HEPA filtered carrier air stream via a sampling tube located 13 cm above the centerline of the burner. The freshly emitted sample was agglomerated in a 5 L aging chamber for ∼30 s. For the case of compact soot discussed below, the soot was passed through a growth tube containing water vapor. The growth tube consisted of a condenser at 10 °C and a hydrator at 45 °C that yielded soot particles embedded within water droplets.[28] The lacey soot particles were then collapsed into a more compact form by removing the water with a pair of diffusion dryers and a tube furnace at 150 °C.[26] Alternatively, the soot could be directed to and removed by a HEPA filter for measurement of particle-free optical background signals.

In the second step, soot size and mass were selected using a tandem differential mobility analyzer (DMA) and aerosol


dx.doi.org/10.1021/es4041804 | Environ. Sci. Technol. 2014, 48, 3169−3176

particle mass analyzer (APM), respectively, as described previously.[6,23] Finally, the soot absorption coefficients ($\alpha_{abs}$) and extinction coefficients ($\alpha_{ext}$) were measured at $\lambda$ = 405 nm using a photoacoustic spectrometer (PA) and a cavity ring-down spectrometer (CRD), respectively, followed by a condensation particle counter (CPC) to yield soot particle number density ($N$). The reader is directed to reviews by Atkinson[29] on cavity ring-down spectroscopy and Haisch[30] on photoacoustic spectroscopy for descriptions of how these techniques are used to measure aerosol optical cross sections. This suite of measurements enabled us to determine the mass-specific extinction and absorption cross sections for both aggregate morphologies. Experimental details can also be found in Radney et al. with specific instrumental details located in the Supporting Information.[6]

Electron microscopy was performed on soot samples using size selected soot that was electrostatically precipitated (TSI 3089, Nanometer aerosol sampler)[31] onto 200-mesh copper TEM grids coated with lacey carbon film at −8 kV collection voltage and a flow of 1.5 L/min. TEM images were collected at an acceleration voltage of 100 kV.

Elemental carbon analysis was performed on lacey soot. Soot particles exiting the agglomeration chamber were collected on quartz fiber filters for 15 s. The elemental carbon to organic carbon (EC/OC) ratio was then measured using an EC/OC analyzer (Sunset Laboratory Dual-Optics Thermal Carbon Analyzer),[31] following the procedure outlined in Conny et al.[32]

**DMA-APM Determination of $D_{fm}$.** The use of a tandem DMA-APM-CPC for measuring particle mass as a function of mobility diameter is well documented and the reader is directed to Ehara et al.[33] or Tajima et al.[34] for a detailed description of this technique. To determine $D_{fm}$, sets of number density and extinction mass distributions were collected as a function of mobility diameter for both lacey and compact soot. This combination of number concentration and extinction allowed for calculation of the distribution of $C_{ext}$ with $m_p$. From this distribution, the singly charged particles of interest were deconvolved from others present; for particles with a $D_m$ of 200 nm or smaller, an additional DMA was required for sufficient resolution. Each distribution was fit using a Gaussian function over the range where only the singly charged particles of interest were present.[6] Additional information on this method is available in the Supporting Information. For each value of $D_m$, we assigned $m_p$ to be the mass value that corresponded to the average mass calculated from these fits. Repeating these measurements over a range of $D_m$ enabled the calculation of $D_{fm}$ from eq 4.

**Measurement Uncertainty.** The reported uncertainties will use our worst-case scenario values of 10% and 5% for cross section and mass, respectively, as determined from multiple measurements spanning several days (see Supporting Information).

**Modeling Soot Optical Properties.** The optical properties of soot were modeled using the superposition T-matrix method.[35−37] The monomer diameters and mean masses were determined from TEM images and APM measurements, respectively. These data enabled us to approximate the number of monomers in each aggregate assuming a monomer mass density of 1.8 g cm$^{-3}$.[38−41] Representative particle morphologies were calculated using cluster−cluster aggregation[42] and diffusion-limited aggregation[43] models for lacey and compact soot, respectively. The $D_f$ and $k_0$ factors were chosen such that the resulting particle morphologies and packing densities agreed well with measured values given below. Using these representative morphologies, a 405 nm wavelength and treating the refractive index as a floating parameter, aggregate absorption and extinction were calculated.

## RESULTS AND DISCUSSION

**Soot Physical Properties.** The measured EC and OC content of freshly generated soot was 68% ± 2% and 31% ± 2%, respectively. For comparison, the OC here is 10% higher than the soot produced in Ferge et al. using a diffusion flame.[44] A representative TEM image of the lacey soot is shown in Figure 2A, revealing the characteristic fractal morphology

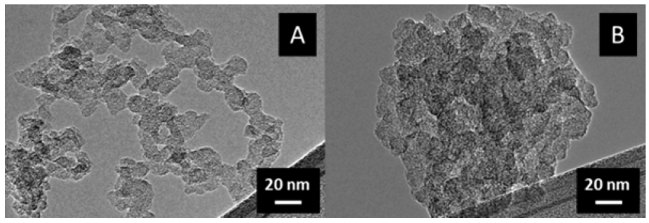


**Figure 2.** TEM images of lacey (A) and compact (B) soot with a mobility diameter of 150 nm.

observed in previous investigations.[39,45] The size distribution of lacey soot was measured and fit to a log-normal distribution and the geometric mean mobility diameter was 116.7 nm with a geometric standard deviation of 1.66. TEM images showed that the soot monomers were 17 ± 2 nm.

A representative TEM image of soot after water uptake and removal is shown in Figure 2B. The structure has collapsed into a nearly spherical shape, with a concomitant reduction in the geometric mean mobility diameter to 106.1 nm and geometric standard deviation to 1.47. Monomer size was unaffected by aggregate collapse.

**Mass Scaling Exponent for Lacey and Compact Soot.** The mass−mobility relationship described by eq 4 was investigated for the lacey and compact soot. The corresponding $m_{p,0}$ and $D_{fm}$ factors are given in Table 1; a summary of data

**Table 1. Mass-Mobility Scaling Fitted Parameters and Uncertainties for Lacey and Compact Soot**

| morphology | $m_{p,0}$ (g) | $\mu(m_{p,0})$ (g) | $D_{fm}$ | $\mu(D_{fm})$ |
|---|---|---|---|---|
| lacey | $3.7 \times 10^{-16}$ | $0.4 \times 10^{-17}$ | 1.76 | 0.08 |
| compact | $3.8 \times 10^{-16}$ | $6 \times 10^{-17}$ | 2.91 | 0.10 |

reduction and analysis can be found in the Supporting Information. A representative set of mobility diameters as a function of mass for both the lacey and compact morphologies were calculated using the mass-mobility scaling relationship and are shown in Table 2. The number of monomers, $N_{mon}$, was calculated using the measured monomer diameter of $D_{mon}$ = 17 nm and an assumed mass density of $\rho$ = 1.8 g cm$^{-3}$.[38−41] The particle packing density ($\theta$) was calculated from the ratio of the spherical volume using the selected mobility diameter and the total volume occupied by the soot via

$$\theta = \frac{N_m D_{mon}^{\ 3}}{D_m^{\ 3}} \quad (5)$$

For values of $m_p$ ranging from $5 \times 10^{-16}$ to $6 \times 10^{-15}$ g, compact soot displays an almost constant packing density near


dx.doi.org/10.1021/es4041804 | Environ. Sci. Technol. 2014, 48, 3169−3176

**Table 2. Representative Mass, Number of Primary Monomers ($D_{mon}$ = 17 nm, $\rho$ = 1.8 g cm$^{-3}$), Mobility Diameters, and Packing Densities of the Lacey and Compact Soot Calculated from the Mass−Mobility Relationship in Table 1**

| | | $D_m$ (nm) | | packing density ($\theta$) | |
|---|---|---|---|---|---|
| $m_p$ ($\times 10^{-15}$ g) | $N_{mon}$ | lacey | compact | lacey | compact |
| 0.5 | 108 | 129 | 113 | 0.25 | 0.37 |
| 1 | 216 | 186 | 142 | 0.16 | 0.37 |
| 2 | 432 | 269 | 180 | 0.11 | 0.37 |
| 3 | 648 | 334 | 206 | 0.09 | 0.36 |
| 4 | 864 | 390 | 227 | 0.07 | 0.36 |
| 5 | 1080 | 439 | 245 | 0.06 | 0.36 |

0.36 ($\rho_{eff} \approx 0.65$ g cm$^{-3}$), while the packing density of the lacey soot decreases from 0.25 to 0.06 ($\rho_{eff} \approx 0.38-0.11$ g cm$^{-3}$, respectively) as $m_p$ increases. Previous work using propane fuel and $H_2SO_4/H_2O$ to induce collapse formed soot with a larger packing density and higher $\rho_{eff}$.[45] In Bueno et al.,[1] soot generated using ethylene fuel collapsed with dibutyl phthalate demonstrated smaller changes in $\rho_{eff}$ than were observed here. These findings indicate that soot collapse may also be affected by the chemical and/or physical properties of the coating material.

**Optical Cross Sections for Lacey and Compact Soot.** The mass-specific absorption and extinction cross sections for both lacey and compact soot were determined from optical cross sections as a function of mass as shown in Figure 3;

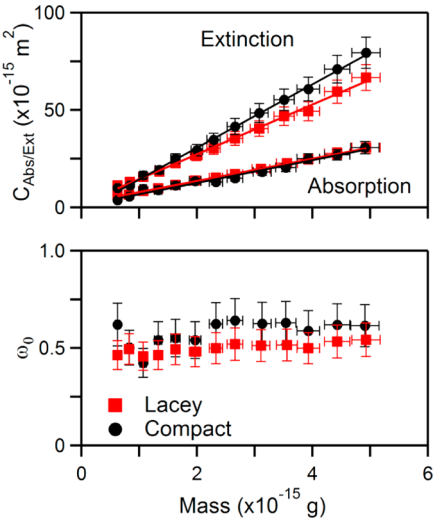


**Figure 3.** Plot of extinction and absorption cross sections versus mass (top) and SSA ($\omega_0$, bottom) for lacey and compact soot. Relative uncertainties ($2\sigma$) are 10% and 5% in cross-section and mass, respectively. SSA errors calculated from propagation of cross-section and mass error.

corresponding MAC and MEC values are shown in Table 3. For comparison to MAC values of other lacey soot measurements, Cross et al.,[2] Zhang et al.,[45] and Slowik et al.[46] obtained 10.0 ± 3.5 m$^2$ g$^{-1}$ at 405 nm, 8.7 m$^2$ g$^{-1}$ at 532 nm (11.4 m$^2$ g$^{-1}$ at 405 nm, $\lambda^{-1}$ dependence), and 6.2 m$^2$ g$^{-1}$ at 870 nm (13.3 m$^2$ g$^{-1}$ at 405 nm, $\lambda^{-1}$ dependence), respectively. Bueno et al.[1] estimated a MAC of 10.9 m$^2$ g$^{-1}$ at 405 nm based upon the work of Zhu et al.[47] The MAC of the soot produced in this study (5.69 ± 0.83 m$^2$ g$^{-1}$) is lower than all of the above-noted

**Table 3. Fit Coefficients and Uncertainties for Lacey and Compact Soot during Extinction and Absorption Measurements**

| measurement | morphology | MAC/MEC (m$^2$ g$^{-1}$) | $\mu$ (m$^2$ g$^{-1}$) | intercept ($10^{-15}$ m$^2$) | $\mu$ ($10^{-15}$ m$^2$) |
|---|---|---|---|---|---|
| extinction | lacey | 12.2 | 1.4 | 2.89 | 2.12 |
| | compact | 15.7 | 1.9 | −0.845 | 2.6 |
| absorption | lacey | 5.69 | 0.83 | 2.22 | 1.35 |
| | compact | 5.97 | 0.73 | 0.50 | 1.4 |

values. This partially arises from the elimination of larger, multiply charged particles presently. Multiply charged particles have larger $C_{abs}$ and relative mass at a given mobility diameter. Failure to completely remove these contributions results in a larger observed MAC. To illustrate this effect, we repeated the above measurements with the inclusion of multiply charged particles (achieved by not using mass selection) and the measured MAC increased to 8.39 ± 1.28 m$^2$ g$^{-1}$ (see Supporting Information), in good agreement with the published work of Bueno et al. using an ethylene fuel source and identical burner design.[1]

The absorption and extinction cross sections vary linearly with particle mass for both the measured morphologies; Bueno et al.[1] observed a similar relationship between absorption cross sections and aggregate volume (and hence mass) for lacey aggregates. The MAC (slope of $C_{abs}$ versus $m_p$) does not exhibit a statistically significant difference for the two morphology cases ($p < 0.01$). This implies that absorption of soot generated in this study correlates primarily with particle mass and is nearly independent of the spatial arrangement of the monomers. We draw this conclusion based upon the additional observations that, within measurement uncertainty, the 150 °C furnace temperature does not alter the amount of EC and OC present in the particle nor the measured optical cross sections (see Supporting Information).

The independence of MAC on morphology observed here can also be rationalized based on the relationship[48]

$$\alpha_{abs,bulk} = \frac{4\pi k}{\lambda} \quad (6)$$

where $\alpha_{abs,bulk}$ is the absorption coefficient of the bulk material and $k$ represents the imaginary component of the refractive index; that is, $n = m + ik$. From the Beer−Lambert law ($I = I_0 e^{-x\alpha_{abs,bulk}}$, where $x$ is distance), the $1/e$ penetration depth of light intensity is $\lambda/4\pi k$. Assuming volume mixing of imaginary components of the refractive indices; that is,

$$k_{eff} = \sum x_i k_i \quad (7)$$

and that the imaginary component of the refractive index is 0.8 (see below for the determination of this value) the penetration depth of the compact soot (0.34% soot, 64% air) is ~110 nm. For the compact particles investigated here, the penetration depth is comparable to the particle radii. Increasing the packing density concomitantly decreases the penetration depth. At maximum random jammed packing (packing density = 64%) the penetration depth decreases to 63 nm and we would expect the observed MAC to be dependent on the particle morphology at the mobility diameters measured.

The experimental findings here are contrary with some modeling results demonstrating a dependence of soot optical properties on morphology; albeit with inconsistent results


dx.doi.org/10.1021/es4041804 | Environ. Sci. Technol. 2014, 48, 3169−3176

within the literature. Liu et al.[17] calculated higher absorption for compact aggregates while Kahnert and Devasthale[18] and Scarnato[19] calculated lower absorption for compact aggregates. However, as noted by Scarnato et al.,[19] monomer diameter relative to the wavelength of light affects modeled MAC morphology dependence; smaller monomers exhibit a cross-over between morphology dependence and independence at shorter wavelengths. In lieu of these observations, we posit the following: in Liu et al.,[17] the modeled packing densities for compact particles ($D_f$ = 2.75 and 3.0) approached the limit of random jammed packing (0.64) and hexagonal close packing (0.74), respectively. The compact soot measured here exhibited a packing density of 0.36, well below those used in the model parameters. Further, the measured monomer diameter (17 nm) is smaller than those used in the above-mentioned studies −30 nm and 50 nm, 50 nm, and 20 nm, respectively, implying that for the soot produced in these experiments at $\lambda$ = 405 nm, a morphology dependence of absorption may not be observed. Lastly, we do not discount the possibility that these results demonstrate a small morphology dependence that is masked by experimental uncertainty.

Unlike the absorption cross section results, the extinction measurements exhibit a statistically significant dependence on particle morphology ($p < 0.01$) consistent with the fact that light scattering (which contributes to extinction) depends strongly on particle shape. Specifically, we find that compact soot has a higher mass-specific extinction cross section (MEC = 15.7 ± 1.9 $m^2$ $g^{-1}$) than the lacey soot (MEC = 12.2 ± 1.4 $m^2$ $g^{-1}$), although both morphologies exhibit a linear relationship between mass and $C_{ext}$, within experimental uncertainty. The observed change in MEC is attributed to the morphological change. Particle compaction with a concomitant increase in $D_f$ and a decrease in the radius of gyration ($R_g$) is expected to result in a 53% increase in MSC for an aggregate with monomers in the Rayleigh regime[16] (see Supporting Information), a value that is nearly identical to the 49% increase in MSC observed for compact soot. Further, it is unlikely that water uptake and removal affects the chemical and optical properties of soot, as we detected no measurable changes in EC/OC below 200 °C and $C_{ext}$ below and 500 °C (see Supporting Information).

The observed variation in extinction cross section leads to a single-scattering albedo $\omega_0$ that depends on soot morphology. We find that $\omega_0$ = 0.50 ± 0.03 and 0.58 ± 0.06 for the lacey and compact soot, respectively, which possess a statistically significant difference ($p < 0.01$). The $\omega_0$ value is significantly higher than the widely referenced BC $\omega_0$ of 0.2 at 550 nm[9] (~0.34 at 405 nm assuming $\lambda^{-1}$ and $\lambda^{-1.64}$ dependence of absorption and extinction, respectively).[2] The findings are attributed to the relatively high organic content of our soot (31% ± 2%). It is well-known that the MAC and $\omega_0$ values of soot tend to decrease and increase, respectively, with increasing organic content because strongly absorbing aromatic constituents correlate with soot EC/OC ratio.[13]

The results demonstrate better agreement when compared to previously published values of soot with comparable organic content. In Schnaiter et al.[14] an $\omega_0$ of 0.43 ± 0.02 at 450 nm was obtained for propane generated soot with 30.2% ± 4.5% OC (see Table 1 in ref 14). Extrapolating $\omega_0$ to 405 nm and assuming the same wavelength dependence as above, a value of 0.53 is obtained. From their data (C/O = 0.40), the MAC and MEC at 405 nm can be estimated as 6 and 11 $m^2$ $g^{-1}$, which exhibit excellent agreement with the values measured for lacey soot in this study.

**Modeling Optical Cross Sections for Lacey and Compact Soot.** The optical cross sections of simulated lacey and compact soot aggregates were calculated using the T-matrix method. The number of monomers in an aggregate was calculated using the measured aggregate mass and an assumed density of 1.8 g $cm^{-3}$ as previously reported.[38−41] Data describing the spatial coordinates of the component monomers were generated using CCA and DLA algorithms for the lacey and compact soot using ($D_f$, $k_0$) of (1.8, 1.6) and (3.0, 0.6), respectively, as described in the Supporting Information. These values were input into the superposition T-matrix method (evaluated assuming $\lambda$ = 405 nm) with the refractive index treated as a floating parameter.

Ideally, we would have treated the refractive index as a fitted parameter; however this approach would have been computationally prohibitive. Alternatively, we considered the following small set of refractive indices guided by literature values and reasonable physical constraints: 1.75 + 0.5$i$,[17] 2 + $i$,[17] 2.1 + 0.9$i$, 2.2 + 0.8$i$, 2.3 + 0.8$i$, 2.4 + 0.8$i$, and 2.4 + 0.7$i$. The first two values, which are representative of literature values for BC, provided good estimates of absorption, but significantly underpredicted the observed extinction. We chose the remaining refractive indices as we do not expect the imaginary component of the refractive index to deviate substantially from previous literature values.[9] Over the values considered, the MAC was relatively insensitive to the choice of complex refractive index, whereas the MEC value was sensitive to the real portion of the refractive index. We found that 2.3 + 0.8$i$ gave the best agreement of MAC and MEC for both morphologies.

Calculated (dashed black line) absorption and extinction cross sections and single scattering albedo as a function of mass using the T-matrix method versus measured values (solid red line with shaded uncertainties as propagated from the linear fits in Table 3) are shown in Figure 4 for lacey soot (left) and compact soot (right). The modeled values were calculated for particles with $N_{mon}$ = 200, 350, 500, 650, and 950.

Figure 4 shows that the T-matrix method captures the linear dependence of absorption (panels A and D) and extinction (panels B and E) cross sections on soot mass for both the lacey and compact morphologies investigated here, respectively. We note that all of the tested refractive indices exhibited a linear dependence of $C_{abs}$ and $C_{ext}$ on mass with the parameter set used. In the case of absorption, the best agreement between model and measurements occurs for the lacey soot (Figure 4A), where average relative deviations in $C_{abs}(m_p)$ of 5% are obtained, with little evidence of systematic deviation. However for the compact soot (Figure 4D), the model systematically overpredicts $C_{abs}(m_p)$ by an average of 14%.

There is qualitative agreement between measured and modeled extinction cross sections which, however, show larger deviations than for particle absorption. Specifically, the calculations predict the extinction cross section to be proportional to soot mass, and yield smaller extinction cross sections for the lacey soot (Figure 4B) than for compact soot (Figure 4E) which is consistent with our observations. However, the calculated extinction cross sections are systematically smaller than the measured values, with average relative deviations of 41.4% and 25.5% for the lacey and compact morphologies, respectively. These deviations indicate that the calculations underestimate the scattering cross sections using


dx.doi.org/10.1021/es4041804 | Environ. Sci. Technol. 2014, 48, 3169−3176

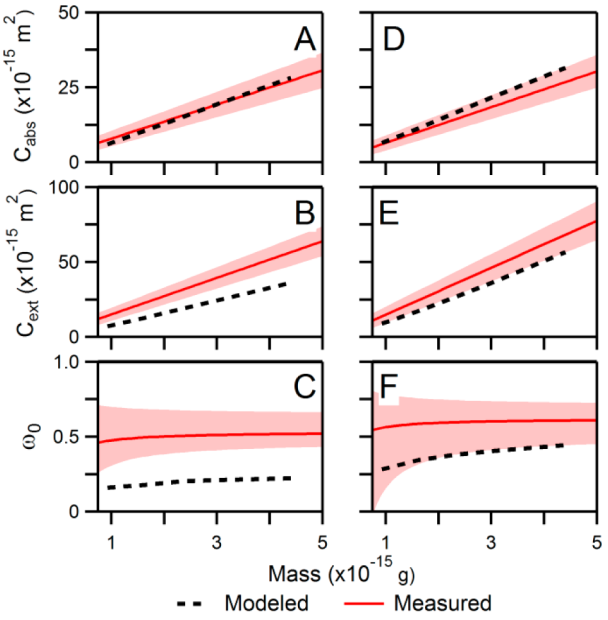


**Figure 4.** Plot of modeled (dashed black line) versus linear fits to measured (solid red line with shaded uncertainties) absorption cross sections, extinction cross sections and single scattering albedo for lacey (A, B, C) and compact soot (D, E, F), respectively versus mass.

the T-matrix method which leads to calculated $\omega_0$ values significantly smaller than the corresponding measured values for both morphology cases (Figures 4C and 4F). Further, $\omega_0$ of the modeled soot displays a stronger mass dependence than the measured soot that arises because the extrapolated intercept for MAC and MEC is nonzero for both the model and measurements, but significantly larger in the model; that is, $C_{abs}$ and $C_{ext} \neq 0$ when $m_p = 0$. The failure to accurately calculate the measured single-scattering albedo may be caused by oversimplification in the model, such as the assumption of fixed-size, primary particles and uniform soot properties throughout the aggregate.

These results are based upon the assumptions that the soot monomers comprise homogeneous 17 nm diameter soot monomers that can be described by a single refractive index. It is possible that the soot monomers possessed a thin organic surface coating that evaporated during TEM imaging. However, from the EC/OC thermograms (see Supporting Information) the soot produced in this study loses less than 1% OC at 200 °C, a temperature above that used to remove water for soot collapse. Assuming all organics were lost during TEM imaging (30% by mass) and have a density of 1 g cm$^{-3}$, results in a 3.5 nm increase in monomer diameter. In the limit of a single monomer, this coating affects the observed cross-section by less than 0.5% if the core is assumed to have a refractive index of 2 + $i$ and the coating has the refractive index of ammonium sulfate (1.53); the refractive index of ammonium sulfate was chosen as it is assumed to be higher than that of any organic that may have been present. In the aggregate limit, if we evaluate $C_{abs}$ and $C_{ext}$ versus mass at a refractive index of 2 + $i$, increasing the monomer diameter from 17 to 25 nm increases these values by 2% and 6%, respectively, while retaining the linear dependence. In running the model using monomer diameters of 34 and 50 nm, the linear dependence of $C_{ext}$ and $C_{abs}$ on mass is lost because of saturation effects. So, while we are omitting potential organic coatings from our model, we do not expect it to significantly alter the observations presented herein.

Although the measured and modeled absorption cross sections discussed here are in good agreement, the results may be improved by incorporation of better physical constraints on any or all of the T-matrix, CCA and DLA input parameters, many of which are interrelated and correlated. Errors in the monomer diameter directly affect the calculated cross sections, but also require modification of $N_{mon}$ and potentially $D_f$ and $k_0$ for a fixed mass. Similarly, errors in mass density affect $N_{mon}$, and potentially $D_f$, $k_0$, and the soot refractive index. A full assessment of small variations within these different parameters to optimize agreement with our measured data is computationally prohibitive and outside the scope of this study.

In conclusion, the mass-specific absorption and extinction coefficients of laboratory-generated soot with lacey and compact morphologies were presented. This study is to our knowledge the first direct comparison of mass-resolved absorption and extinction cross sections with theoretical calculations based on the superposition T-matrix method of light scattering and absorption. The observed mass-specific absorption cross sections were nominally independent of particle morphology (5.69 ± 0.83 and 5.97 ± 0.73 m$^2$ g$^{-1}$ for the lacey and compact soot, respectively) and low when compared to the commonly cited BC value of 7.5 ± 1.2 m$^2$ g$^{-1}$ at $\lambda$ = 550 nm (10.2 ± 1.63 m$^2$ g$^{-1}$ at 405 nm, $\lambda^{-1}$ dependence).[9] When compared to soot aerosol with similar OC content[14] or when neglecting the contribution of multiply charged particles,[2] better MAC agreement was obtained. The corresponding extinction cross sections were much more sensitive to morphology (12.2 ± 1.4 and 15.7 ± 1.9 m$^2$ g$^{-1}$ for the lacey and compact soot, respectively) and also agree well with soot aerosol with comparable OC content.[14] The measurements are contrary to recent modeling studies where both MAC and MEC displayed morphology dependence; however, these other modeling studies used soot with larger monomer diameters and higher effective densities than those measured in this study.[17−19] The model predictions qualitatively demonstrate the measured morphology independence of absorption and dependence of extinction. Better numerical agreement between measurements and calculations could be obtained by constraining the physical parameters describing the system better or using a model that can treat soot monomers as having a heterogeneous composition and size distribution.

## ■ ASSOCIATED CONTENT

### Supporting Information

Additional information regarding the theory of operation of the DMA, APM, CRD, and PAS, details on the isolation of the +1 charge soot peak from mass distributions, the corresponding mass-mobility relationship, the observed MAC without mass selection, measurement uncertainty of our instrumentation, soot variability, the dependence of soot composition and cross-section on temperature, determination of scattering enhancement for aggregates in the Rayleigh regime, and the calculation of lacey and compact soot aggregate structures using CCA and DLA, respectively. This information is available free of charge via the Internet at http://pubs.acs.org/.

## AUTHOR INFORMATION


### Corresponding Author

*E-mail: cdzang@nist.gov. Phone: (301) 975-8709. Fax: (301) 975-3670.


### Author Contributions

The manuscript was written through contributions of all authors. All authors have given approval to the final version of the manuscript.

### Notes

The authors declare no competing financial interest.

## SYMBOLS

| | |
|---|---|
| $\alpha_{abs}$ | absorption coefficient, $m^{-1}$ |
| $\alpha_{ext}$ | extinction coefficient, $m^{-1}$ |
| $\alpha_{sca}$ | scattering coefficient, $m^{-1}$ |
| $C_{abs}$ | absorption cross section, $m^2$ |
| $C_{sca}$ | scattering cross section, $m^2$ |
| $C_{ext}$ | extinction cross section, $m^2$ |
| $D_f$ | fractal dimension |
| $D_{fm}$ | mass-mobility scaling exponent |
| $D_m$ | electrical mobility diameter, nm |
| $D_{m,0}$ | initial mobility diameter in mass-mobility scaling relationship, nm |
| $D_{mon}$ | monomer diameter, nm |
| $k_0$ | fractal prefactor |
| $k$ | imaginary refractive index |
| $\lambda$ | wavelength, nm |
| $m_p$ | particle mass, g |
| $m_{p,0}$ | initial mass in mass-mobility scaling relationship, g |
| MAC | mass specific absorption cross section, $m^2\ g^{-1}$ |
| MEC | mass specific extinction cross section, $m^2\ g^{-1}$ |
| MSC | mass specific scattering cross section, $m^2\ g^{-1}$ |
| $N$ | number density, $m^{-3}$ |
| $N_{mon}$ | number of monomers |
| $\theta$ | packing density |
| $R_g$ | radius of gyration, nm |
| $\omega_0$ | single scattering albedo |

## REFERENCES


(1) Bueno, P. A.; Havey, D. K.; Mulholland, G. W.; Hodges, J. T.; Gillis, K. A.; Dickerson, R. R.; Zachariah, M. R. Photoacoustic Measurements of Amplification of the Absorption Cross Section for Coated Soot Aerosols. *Aerosol Sci. Technol.* **2011**, *45* (10), 1217−1230.

(2) Cross, E. S.; Onasch, T. B.; Ahern, A.; Wrobel, W.; Slowik, J. G.; Olfert, J.; Lack, D. A.; Massoli, P.; Cappa, C. D.; Schwarz, J. P.; Spackman, J. R.; Fahey, D. W.; Sedlacek, A.; Trimborn, A.; Jayne, J. T.; Freedman, A.; Williams, L. R.; Ng, N. L.; Mazzoleni, C.; Dubey, M.; Brem, B.; Kok, G.; Subramanian, R.; Freitag, S.; Clarke, A.; Thornhill, D.; Marr, L. C.; Kolb, C. E.; Worsnop, D. R.; Davidovits, P. Soot Particle Studies—Instrument Inter-Comparison—Project Overview. *Aerosol Sci. Technol.* **2010**, *44* (8), 592−611.

(3) Radney, J. G.; Bazargan, M. H.; Wright, M. E.; Atkinson, D. B. Laboratory Validation of Aerosol Extinction Coefficient Measurements by a Field-Deployable Pulsed Cavity Ring-Down Transmissometer. *Aerosol Sci. Technol.* **2009**, *43* (1), 71−80.

(4) Lack, D. A.; Lovejoy, E. R.; Baynard, T.; Pettersson, A.; Ravishankara, A. R. Aerosol Absorption Measurement using Photoacoustic Spectroscopy: Sensitivity, Calibration, and Uncertainty Developments. *Aerosol Sci. Technol.* **2006**, *40* (9), 697−708.

(5) Abo Riziq, A.; Erlick, C.; Dinar, E.; Rudich, Y. Optical Properties of Absorbing and Non-absorbing Aerosols Retrieved by Cavity Ring down (CRD) Spectroscopy. *Atmos. Chem. Phys.* **2007**, *7* (6), 1523−1536.

(6) Radney, J. G.; Ma, X.; Gillis, K. A.; Zachariah, M. R.; Hodges, J. T.; Zangmeister, C. D. Direct Measurements of Mass-Specific Optical Cross Sections of Single Component Aerosol Mixtures. *Anal. Chem.* **2013**, *85* (17), 8319−8325.

(7) Sato, M.; Hansen, J.; Koch, D.; Lacis, A.; Ruedy, R.; Dubovik, O.; Holben, B.; Chin, M.; Novakov, T. Global Atmospheric Black Carbon Inferred from AERONET. *Proc. Natl. Acad. Sci. U.S.A.* **2003**, *100* (11), 6319−6324.

(8) Buseck, P. R.; Adachi, K.; Gelencsér, A.; Tompa, É.; Pósfai, M. Are black Carbon and Soot the Same? *Atmos. Chem. Phys. Discuss.* **2012**, *12* (9), 24821−24846.

(9) Bond, T. C.; Bergstrom, R. W. Light Absorption by Carbonaceous Particles: An Investigative Review. *Aerosol Sci. Technol.* **2006**, *40* (1), 27−67.

(10) *Climate Change 2007: The Physical Science Basis*, Contribution of Working Group I to the Fourth Assessment Report of the Intergovernmental Panel on Climate Change; Solomon, S. D., Qin, M. M., Chen, Z., Marquis, M., Averyt, K. B., Tignor, M., Miller, H. M., Eds.; Cambridge University Press: Cambridge, U.K., 2007; p 996.

(11) In *Aerosol Forcing of Climate*, Dahlem Workshop on Aerosol Forcing of Climate, Berlin, 1994; Charlson, R. J., Heintzenberg, J., Eds.; John Wiley & Sons: Berlin, 1994.

(12) Ishiguro, T.; Takatori, Y.; Akihama, K. Microstructure of Diesel Soot Particles Probed by Electron Microscopy: First Observation of Inner Core and Outer Shell. *Combust. Flame* **1997**, *108* (1−2), 231−234.

(13) Widmann, J. F.; Yang, J. C.; Smith, T. J.; Manzello, S. L.; Mulholland, G. W. Measurement of the Optical Extinction Coefficients of Post-Flame Soot in the Infrared. *Combust. Flame* **2003**, *134* (1−2), 119−129.

(14) Schnaiter, M.; Gimmler, M.; Llamas, I.; Linke, C.; Jäger, C.; Mutschke, H. Strong Spectral Dependence of Light Absorption by Organic Carbon Particles Formed by Propane Combustion. *Atmos. Chem. Phys.* **2006**, *6* (10), 2981−2990.

(15) Heidenreich, R. D.; Hess, W. M.; Ban, L. L. A Test Object and Criteria for High Resolution Electron Microscopy. *J. Adv. Phytochem. Res.* **1968**, *1*, 1−19.

(16) Sorensen, C. M. Light Scattering by Fractal Aggregates: A Review. *Aerosol Sci. Technol.* **2001**, *35* (2), 648−687.

(17) Liu, L.; Mishchenko, M. I.; Patrick Arnott, W. A Study of Radiative Properties of Fractal Soot Aggregates Using the Superposition T-Matrix Method. *J. Quant. Spectrosc. Radiat. Transfer* **2008**, *109* (15), 2656−2663.

(18) Kahnert, M.; Devasthale, A. Black Carbon Fractal Morphology and Short-Wave Radiative Impact: A Modelling Study. *Atmos. Chem. Phys.* **2011**, *11* (22), 11745−11759.

(19) Scarnato, B. V.; Vahidinia, S.; Richard, D. T.; Kirchstetter, T. W. Effects of Internal Mixing and Aggregate Morphology on Optical Properties of Black Carbon Using a Discrete Dipole Approximation Model. *Atmos. Chem. Phys.* **2013**, *13* (10), 5089−5101.

(20) Mountain, R. D.; Mulholland, G. W. Light Scattering from Simulated Smoke Agglomerates. *Langmuir* **1988**, *4* (6), 1321−1326.

(21) Heinson, W. R.; Sorensen, C. M.; Chakrabarti, A. Does Shape Anisotropy Control the Fractal Dimension in Diffusion-Limited Cluster-Cluster Aggregation? *Aerosol Sci. Technol.* **2010**, *44* (12), i−iv.

(22) Park, K.; Kittelson, D.; McMurry, P. Structural Properties of Diesel Exhaust Particles Measured by Transmission Electron Microscopy (TEM): Relationships to Particle Mass and Mobility. *Aerosol Sci. Technol.* **2004**, *38*, 881−889.

(23) Park, K.; Cao, F.; Kittelson, D. B.; McMurry, P. H. Relationship between Particle Mass and Mobility for Diesel Exhaust Particles. *Environ. Sci. Technol.* **2003**, *37* (3), 577−583.

(24) Scheckman, J. H.; McMurry, P. H.; Pratsinis, S. E. Rapid Characterization of Agglomerate Aerosols by In Situ Mass−Mobility Measurements. *Langmuir* **2009**, *25* (14), 8248−8254.

(25) Eggersdorfer, M. L.; Kadau, D.; Herrmann, H. J.; Pratsinis, S. E. Aggregate Morphology Evolution by Sintering: Number and Diameter of Primary Particles. *J. Aerosol Sci.* **2012**, *46* (0), 7−19.

(26) Ma, X.; Zangmeister, C. D.; Gigault, J.; Mulholland, G. W.; Zachariah, M. R. Soot Aggregate Restructuring during Water Processing. *J. Aerosol Sci* **2013**, *66* (0), 209−219.
(27) Santoro, R. J.; Semerjian, H. G.; Dobbins, R. A. Soot Particle Measurements in Diffusion Flames. *Combust. Flame* **1983**, *51* (0), 203−218.
(28) Hering, S. V.; Stolzenburg, M. R. A Method for Particle Size Amplification by Water Condensation in a Laminar, Thermally Diffusive Flow. *Aerosol Sci. Technol.* **2005**, *39* (5), 428−436.
(29) Atkinson, D. B. Solving Chemical Problems of Environmental Importance Using Cavity Ring-down Spectroscopy. *Analyst* **2003**, *128* (2), 117−125.
(30) Haisch, C. Photoacoustic Spectroscopy for Analytical Measurements. *Meas. Sci. Technol.* **2012**, *23* (1), 012001.
(31) NIST Technical Disclaimer: Certain commercial equipment, instruments, or materials (suppliers, software, etc.) are identified in this paper to foster understanding. Such identification does not imply recommendation or endorsement by the National Institute of Standards and Technology, nor does it imply that the materials or equipment identified are necessarily the best available for the purpose.
(32) Conny, J. M.; Norris, G. A.; Gould, T. R. Factorial-Based Response-Surface Modeling with Confidence Intervals for Optimizing Thermal−Optical Transmission Analysis of Atmospheric Black Carbon. *Anal. Chim. Acta* **2009**, *635* (2), 144−156.
(33) Ehara, K.; Hagwood, C.; Coakley, K. J. Novel Method to Classify Aerosol Particles According to Their Mass-to-Charge Ratio—Aerosol Particle Mass Analyser. *J. Aerosol Sci* **1996**, *27* (2), 217−234.
(34) Tajima, N.; Fukushima, N.; Ehara, K.; Sakurai, H. Mass Range and Optimized Operation of the Aerosol Particle Mass Analyzer. *Aerosol Sci. Technol.* **2011**, *45* (2), 196−214.
(35) Mackowski, D. W. *MSTM: A Multiple Sphere T-Matrix FORTRAN Code for Use on Parallel Computer Clusters*, version 2.2; Goddard Institute for Space Studies, National Aeronautics and Space Administration: New York, 2011.
(36) Mackowski, D. W. *MSTM: A Multiple Sphere T-Matrix FORTRAN Code for Use on Parallel Computer Clusters*, version 3.0; Goddard Institute for Space Studies, National Aeronautics and Space Administration: New York, 2013.
(37) Mackowski, D. W.; Mishchenko, M. I. A Multiple Sphere T-Matrix Fortran Code for Use on Parallel Computer Clusters. *J. Quant. Spectrosc. Radiat. Tranfer* **2011**, *112* (13), 2182−2192.
(38) Park, K.; Kittelson, D.; Zachariah, M.; McMurry, P. Measurement of Inherent Material Density of Nanoparticle Agglomerates. *J. Nanopart. Res.* **2004**, *6* (2), 267−272.
(39) Adler, G.; Riziq, A. A.; Erlick, C.; Rudich, Y. Effect of Intrinsic Organic Carbon on the Optical Properties of Fresh Diesel Soot. *Proc. Natl. Acad. Sci. U.S.A.* **2010**, *107* (15), 6699−6704.
(40) Schwarz, J. P.; Gao, R. S.; Fahey, D. W.; Thomson, D. S.; Watts, L. A.; Wilson, J. C.; Reeves, J. M.; Darbeheshti, M.; Baumgardner, D. G.; Kok, G. L.; Chung, S. H.; Schulz, M.; Hendricks, J.; Lauer, A.; Kärcher, B.; Slowik, J. G.; Rosenlof, K. H.; Thompson, T. L.; Langford, A. O.; Loewenstein, M.; Aikin, K. C. Single-Particle Measurements of Midlatitude Black Carbon and Light-Scattering Aerosols from the Boundary Layer to the Lower Stratosphere. *J. Geophys. Res.: Atmos.* **2006**, *111* (D16), D16207.
(41) Schkolnik, G.; Chand, D.; Hoffer, A.; Andreae, M. O.; Erlick, C.; Swietlicki, E.; Rudich, Y. Constraining the Density and Complex Refractive Index of Elemental and Organic Carbon in Biomass Burning Aerosol Using Optical and Chemical Measurements. *Atmos. Environ.* **2007**, *41* (5), 1107−1118.
(42) Jullien, R.; Botet, R.; Mors, P. M. Computer Simulations of Cluster−Cluster Aggregation. *Faraday Discuss.* **1987**, *83* (0), 125−137.
(43) Meakin, P. Computer Simulations of Diffusion-Limited Aggregation Processes. *Faraday Discuss.* **1987**, *83* (0), 113−124.
(44) Ferge, T.; Karg, E.; Schroppel, A.; Coffee, K. R.; Tobias, H. J.; Frank, M.; Gard, E. E.; Zimmermann, R. Fast Determination of the Relative Elemental and Organic Carbon Content of Aerosol Samples by On-Line Single-Particle Aerosol Time-of-Flight Mass Spectrometry. *Environ. Sci. Technol.* **2006**, *40* (10), 3327−35.
(45) Zhang, R.; Khalizov, A. F.; Pagels, J.; Zhang, D.; Xue, H.; McMurry, P. H. Variability in Morphology, Hygroscopicity, and Optical Properties of Soot Aerosols during Atmospheric Processing. *Proc. Natl. Acad. Sci. U.S.A.* **2008**, *105* (30), 10291−10296.
(46) Slowik, J. G.; Cross, E. S.; Han, J.-H.; Davidovits, P.; Onasch, T. B.; Jayne, J. T.; Williams, L. R.; Canagaratna, M. R.; Worsnop, D. R.; Chakrabarty, R. K.; Moosmüller, H.; Arnott, W. P.; Schwarz, J. P.; Gao, R.-S.; Fahey, D. W.; Kok, G. L.; Petzold, A. An Inter-Comparison of Instruments Measuring Black Carbon Content of Soot Particles. *Aerosol Sci. Technol.* **2007**, *41* (3), 295−314.
(47) Zhu, J.; Choi, M. Y.; Mulholland, G. W.; Gritzo, L. A. Measurement of Soot Optical Properties in the near-Infrared Spectrum. *Int. J. Heat Mass Transfer* **2000**, *43* (18), 3299−3303.
(48) Bohren, C. F.; Huffman, D. R. *Absorption and Scattering of Light by Small Particles*; Wiley: New York, 1983.